NATIONAL INSTITUTE FOR FUSION SCIENCE

A Simple Theoretical Approach to
Determine Relative Ion Yield (RIY) in
Glow Discharge Mass Spectrometry (GDMS)

S. Born, N. Matsunami and H. Tawara

RESEARCH REPORT
NIFS-DATA Series

NAGOYA, JAPAN

A simple theoretical approach to determine relative ion yield (RIY) in glow discharge mass spectrometry (GDMS)

Sabine Born*, Noriaki Matsunami** and Hiroyuki Tawara***

*Degussa AG, 63403 Hanau, Germany
**Energy Engineering and Science, Engineering, Nagoya University,
Furo-cho, Chikusa-ku, Nagoya 464-8603, Japan
***National Institute for Fusion Science, Toki, 509-5259, Japan

Abstract

Direct current glow discharge mass spectrometry (dc-GDMS) has been applied to detect impurities in metals. The aim of this study is to understand quantitatively the processes taking place in GDMS and establish a model to calculate the relative ion yield (RIY), which is inversely proportional to the relative sensitivity factor (RSF), in order to achieve better agreement between the calculated and the experimental RIYs. A comparison is made between the calculated RIY of the present model and the experimental RIY, and also with other models.

1. Introduction

The direct current glow discharge mass spectrometry (dc-GDMS) is known to be a powerful tool of detecting impurities in conducting solid materials (see reviews [1,2]). Basically, in GDMS, the secondary ions from the target are analyzed. GDMS has high detection efficiencies, usually in ppb (ng/g) or sub-ppb range for nearly all the elements. The concentration ratio C_X/C_S of the impurity over the matrix is related with the ratio of the impurity ion current (I_X) over the matrix ion current (I_S) measured in GDMS,

$$I_X/I_S = RIY \cdot (C_X/C_S)$$
$$= (C_X/C_S)(M_X/M_S)/RSF. \quad (1)$$

Where RIY is so-called relative ion yield, RSF is the relative sensitivity factor, and M_X and M_S are the masses of impurity and matrix ions. RIY can be determined experimentally using certified reference material with the known impurity concentration and its value is generally order of unity. Because the reference materials for all impurity/material combinations are not always available, it is desirable to predict RIY with model calculations. So far, agreement of the calculated RIY with the experimental RIY is not satisfactory, in spite of extensive studies by Bogaerts and Gijbels [3], Bogaerts [4], and Vieth and Huneke [5,6].

The aim of the present study is to understand quantitatively the processes taking place in GDMS and establish a model to calculate RIY to achieve better agreement with the experimental RIY. We compare the calculated RIY of our model with the experimental RIY and also with other model. In the plasma, there exist a variety of plasma species, i.e., electrons, neutral atoms,

ions, their excited species and various kinds of clusters. These species collide with each other, leading to complicated processes. In the present study, we consider that the following processes play roles in the glow-discharge (GD) plasma cell:
(1) Sputtering of target by positive ions accelerated by the electric field near the cathode,
(2) Transport of sputtered neutral atoms to anode,
(3) Ionization of sputtered neutral atoms near the anode,
(4) Extraction of ions generated near the anode to the lens and magnetic analyser. These processes of (1) to (4) will be discussed in details after a description of the experimental.

2. Experimental

A schematics of glow discharge is shown in Fig. 1 [1]. The experiments were carried out using a VG9000. The GD plasma cell consists of an anode housing of 25 mm in diameter and a cathode disk with an electrical insulation of boron nitride and about 1 kV is applied between them. The cathode is separated by 10 mm from the anode slit. The central part of the cathode of 10 mm in diameter is the target to be analyzed, viz., the reference material which consists of a metal matrix with a trace impurity. The impurity concentration in the reference material has been determined within an accuracy of ~1 % by wet chemical analysis such as inductively-coupled-plasma mass-spectrometry (ICP-MS) [7]. Typical discharge current is 1–10 mA in Ar gas of ~ 100 Pa (~ 1 Torr). Only a fraction of 10^{-3} to 10^{-4} of Ar atoms is estimated to be ionized in a typical GD [1]. Eckstein, Coburn and Kay [8] reported that the

ionized fraction is ~ 10^{-4} for Ne gas GD. Ar^+ ions are accelerated by the fields near the cathode and the target (cathode) are subject to these ion bombardment, resulting in sputtering of matrix and impurity atoms (see a review by Behrish [9]). The anode potential is kept at about 8 kV against the ground and ions generated near the anode are extracted through the anode slit and led to the ion mass analyser.

3. A theoretical model

3.1 Relative ion yield (RIY)

As discussed in § 1, RIY can be written in terms of the relative sputtering yield of impurity to that of matrix for $C_X/C_S = 1$ (RS), the relative transport efficiency of sputtered neutral impurity atoms to that of matrix atoms (RT), the relative ionization probability of impurity to that of matrix atoms (RI) and the relative extraction efficiency of impurity ions to that of matrix ions (RE):

$$RIY = RS \cdot RT \cdot RI \cdot RE. \quad (2)$$

Some physical constants relevant to RIY calculation are given in Appendix A.

3.2 Sputtering

The sputtering yield (atoms per ion) of monatomic targets by ion impact can be estimated from simulations such as TRIM by Ziegler, Biersack and Littmark [10], and semi-empirical formulae by Matsunami et al. [11] and by Yamamura and Tawara [12], using the surface binding energies and densities given in Appendix A. Firstly, the energy of Ar^+ ions involved in GD is discussed. Under the conditions stated above, Ar^+ ions can gain the maximum of 1 keV. Measurements by Straaten, Bogaerts and Gijbels [13] indicate that the average energy of Ar^+ ions is 0.1 to 0.15 keV at Ar gas pressure of 50 to 100 Pa and the discharge currents of 1 to 3 mA. The erosion rate of the cathode appeared to be independent of the discharge current [14,15], indicating that no melting process takes place and target erosion is not due to evaporation but sputtering by ion impact. Using a typical size of the observed crater for Cu target (3.3×10^{-3} cm^3 at discharge current of 5 mA for 2 hr [14]), the erosion rate was estimated as 2.5 (Cu atoms per ion), assuming that a half of the discharge current is due to Ar^+ and the rest is the electron current. The angle of incidence measured from the target surface normal (θ) of the Ar^+ ions is estimated to range from $\theta = 0$ to $\theta_m = \sim 80$ degrees in view of the GDMS geometry. Hence, the sputtering yield of the target atoms can be enhanced by a factor of 1.74 at $\theta_m=80$ over that at normal incidence, assuming an uniform angular distribution of incidence and the $1/\cos(\theta)$ law of sputtering [9]. Comparing the erosion

rate with the calculated sputtering yield of TRIM (1997 version), the Ar^+ energy is estimated as ~0.3 keV. The discrepancy could be partly due to the re-sputtering and an error in the estimation of Ar^+ current. The energetic neutral Ar atoms may contribute to the sputtering. In the present study, the energy of Ar^+ in GDMS is assumed to be around 0.15 keV. RIY is not seriously sensitive to the choice of the energy.

It is worthwhile to compare the sputtering yields of the computer simulation (TRIM97) with those of experiments which are taken from the references listed in the data compilation [11,12] (Fig. 2). For most of the elements, agreement of the sputtering yields between the simulation and experiments is within a factor of 2, except for low energies. For Si, the simulation values are somewhat smaller. For Be, the simulation values underestimate significantly, especially for low energies. It also appears that the simulated sputtering yields of C are smaller than those of experiments by a factor of 8 to 4 at 0.15 to 0.5 keV. These imply that the TRIM97 simulation underestimates the sputtering yields significantly for low z elements such as Be, B and C. The semi-empirical values at 0.1, 0.15 and 0.5 keV by Yamamura and Tawara [12] are 0.02, 0.074 and 0.443 for B, 1.1, 1.54 and 3.23 for Na, and 0.73, 1.06 and 2.38 for Mg, respectively. We use the experimental values for Be and Si, the semi-empirical values for B, Na and Mg, and the TRIM97 simulation values for other elements than Be, B, Na, Mg and Si. The sputtering yields S of elemental targets by 150 eV Ar impact at normal incidence are given in Appendix A.

Now, the sputtering of alloys, i.e., multi-component targets, is discussed. Sputtering yields of each component in alloys cannot be simply estimated from those of elemental targets because of modifications of the compositions near surface (called segregation), of the surface binding energies and of the elastic energy depositions (see a ref. by Shimizu [16]). Thus one of the components can be selectively (preferentially) sputtered, generating the altered layer, where the composition differs from that of the bulk. The selective sputtering continues until the steady state is reached. After the steady state is reached, the sputtering yields of each component become equal to those of the bulk composition. Hence, in the first approximation, the relative sputtering yield RS is given by,

$$RS = 1. \quad (3)$$

In this case, the energy of Ar responsible for target sputtering does not play a role at all. Equation (3) has been supported by the fact that RIY is kept unchanged for a prolong discharge time [14] and, though it has not been confirmed yet, eq.(3) sounds good, unless the steady state condition is violated. Extensive theoretical studies based on the above equation by Bogaerts and

Gijbels [3], Bogaerts [4], and Vieth and Huneke [5,6], however, did not give satisfactory agreement with the experimental RIY. This could be largely due to poor understanding of ionization, transport, extraction efficiencies. Nevertheless, the above situation leads us to modify eq.(3) and such a trial is discussed.

In dilute alloys ($C_X \ll C_S$), it is reasonable to assume that the surface binding energy (U_X) of impurity is the same as that of the matrix (U_S), ignoring the selective sputtering. A crude assumption that the elastic-energy-deposition cross section per atom in the elemental target is the same as in the two-component target would give a possible modification, reminding that the sputtering yield is inversely proportional to the surface binding energy.

$$RS = (U_X/U_S) \cdot (S_X/S_S), \qquad (4)$$

where S_X and S_S are the sputtering yield of one-component target consisting of impurity and that of matrix atoms, respectively (Appendix A). It appears that this choice improves slightly the agreement between the calculated and experimental RIY for certain cases (probably fortuitous), noticing that it is difficult to find a good physical meaning of eq.(4). In this case, again, the energy of Ar for target sputtering is insignificant, because RS calculated by TRIM97 is relatively insensitive to the Ar^+ energy as shown in Fig. 3 for Cu matrix. The variation of RS with the Ar^+ energy is within ~20 % for 0.1 to 0.5 keV, except for B and Be. The ratio at 50 eV is somewhat larger or smaller than that at 0.1 to 0.5 keV. The variation for B and Be could be more than a factor of 2. The situation is quite similar to other matrices (Al, Ti, Fe, Zn, Ag, Sn, Au, Pb).

3.3 Transport of neutral atoms from the cathode to anode

Some of the sputtered neutral atoms from the cathode are ionized in the negative glow and the positive column regions. However, these positive ions feel the weak electric field towards the cathode and cannot reach the anode. Vieth and Huneke [6], and Bogaerts and Gijbels [3] assumed that the transport efficiency of the sputtered atoms is inversely proportional to the diffusivity D_X and that $1/D_X \propto (r_X + r_{Ar})^2 (\mu_X)^{1/2}$. Here, r_X and r_{Ar} are the atomic radii of the impurity and Ar, respectively, and $(r_X + r_{Ar})^2$ represents the cross section of collisions between the sputtered atom and Ar atom, and μ_X is the reduced mass of impurity atom and Ar, $\mu_X = M_X M_{Ar}/(M_X + M_{Ar})$. Remind that within the hard

sphere model, the collision cross section is independent of the energy of sputtered atoms. Hence, the collisions of the sputtered atoms with Ar atoms are frequent enough so that the transport of the sputtered atoms can be treated by a diffuison process, and that the initial angular and energy distributions of the sputtered atoms are no longer kept when the sputtered atoms reach the anode and the effect can be discarded. Then the relative transport efficiency (RT) is given by

$$RT = (\mu_X / \mu_S)^{1/2} \{(r_X + r_{Ar})/(r_S + r_{Ar})\}^2. \quad (5)$$

Note that more stronger dependence on the atomic radius (4th-power of the radius sum instead of the 2nd-power) is suggested by Hang and Harrison [17] for transport of neutral atoms.

In this study, the atomic radii (r) are taken as the calculated mean atomic radii of the outer shells (relativistic Hartree-Fock-Slater calculation) [18], neglecting d- and f-shell contributions and the values are given in Appendix A. The radius of Pd is taken as the mean of the radii of the neighbouring two atoms (Rh and Ag), because Pd has no 5s-electron but filled 4d-electron and the 4d-shell radius is too small to be the atomic radius. These calculated values (Appendix A) agree to an accuracy of 10% with the radii of 12-coordinated or tetrahedral covalent configurations [19], except that the calculated values are larger by more than 20% for Li and Be and larger by up to ~50% for those atoms having d-shell contributions (Sc to Cu, Y to Ag and Lu to Pt), and smaller by a factor of ~ 2 for inert gas atoms (Ne, Ar, Kr and Xe). The radii of the atoms having the d-shell contributions agree within ~ 10% with those in ref. [19], by taking an appropriate averaging of the outer shell radii [20]. The calculated RT (eq.(5)) ranges from 0.4 to 2.2 for Fe matrix as given in Table 1 and these values differ by 10~30 % from the values in ref. [3] (for Sb, the difference is the maximum of -34%). These discrepancies are probably due to the choice of the atomic radii. In fact, usage of atomic radii from ref. [19] gives RT values closer to those in ref. [3] for many impurities within ~10%, except for Na, Si, Ca, As, In and Pb, the difference being the maximum of 17 % for Ca.

3.4 Ionization of atoms near the anode

A part of neutral atoms reached near the anode are ionized. Then the ions are extracted through a slit of the anode, sent into the lens system and ion mass analyser, and finally reach a detector. There are two mechanisms of ionization: Electron impact ionization (EI) and Penning ionization (PI) (see a review by Siska [21] for PI).

3.4.1. Electron impact ionization

In the case that EI is dominant for ionization, we need to know the electron energy (distribution) to estimate EI cross section (EICS). According to the calculation by Bogaerts [4], the electron reaches the energy of 0.5 keV and has a flat distribution down to several eV (secondary electron region). The electron acceleration presumably takes place very near the cathode (cathode dark space) and the electrons lose their energy in the negative glow (NG) and/or positive column before reaching the anode. The total energy loss of an electron with the energy of 0.5 - 0.3 keV in Ar at 100 Pa is calculated as ~0.2 keV/cm (ICRU84 report [22]). It is interesting to compare this value with that of the above calculation [4]. The energy loss of charged particles (electrons and ions) in plasma is also an interesting subject.

The relative electron-impact ionization probability of impurity to that of matrix (REI) is simply given by

$$REI = \sigma_{XEI}(Ee) / \sigma_{SEI}(Ee) , \qquad (6)$$

where, σ_{XEI} and σ_{SEI} are the electron impact ionization cross sections (EICS) for impurities and matrix at an electron energy of Ee. EICS for many elements are given by Bell et al. [23], Lennon et al. [24], Higgings et al. [25], and Tawara [26]. Data from Tawara are used for all elements investigated in this study, except for Sn. For Sn, EICS is taken from ref. Higgins et al. [25]. EICS at the electron energy of 100 eV together with the ionization potential I are given in Appendix A. EICS data for Sb, Bi, Pd, Rh and Pt are not available at present. EICS for Au seems to be a little bit larger [26] and the values are not used in the following REI calculation. REI has a weak energy dependence as shown in Figs. 4(a) and (b). From these results and the fact that the calculated energy of electrons is less than 0.5 keV and order of 0.1 keV as mentioned above, the electron energy for EICS is chosen as 100 eV in this study. Averaging of the EICS is not significant, unless the electron energy is lower than ~ 50 eV. To improve the accuracy, the EICS should be averaged over the electron energy distribution, if it is known.

3.4.2 Penning ionization

There is an estimation by Smith, Serxner and Hess [27] that Penning ionization (PI) contribution is ~ 50 %. There are a few data on the PI cross section, σ_{PI} (Riseberg, Parks and Schearer [28]). The ratio of PI over EI contributions can be estimated by

$$< \sigma_{PI} \cdot N(Ar^*) \cdot v> / < \sigma_{EI} \cdot Je> , \qquad (7)$$

where $N(Ar^*)$ is the Ar metastable density, v the relative velocity of atoms to be ionized and Ar^*, and Je the electron current density. $<>$ means averaging over v. Inserting $\sigma_{PI} / \sigma_{EI} \sim 10$, $v \sim 10^5$ cm/s (corresponding to ~1eV Ar), $Je \sim 10^{16}$/cm^{2}s (~1mA/cm^2), Eq.(7) becomes larger than unity when $N(Ar^*)/N(Ar) > 10^{-6}$ for 100 Pa Ar ($N(Ar) \sim 3.5 \times 10^{16}$/cm^3), indicating that PI is dominant. Hence, data of σ_{PI} and $N(Ar^*)$ are of crucial importance for evaluation of the PI contribution.

An approximate formula for the relative Penning ionization of impurity to that of matrix atoms (RPI) is given by Riseberg, Parks and Schearer [28], assuming that σ_{PI} is proportional to $\pi \mu^{1/2} r^3$ ($\sigma_{PI} \propto$ polarizability $\propto r^3$) ,

$$RPI = (\mu_X / \mu_S)^{1/2} (r_X / r_S)^3 , \qquad (8)$$

where μ is the reduced mass defined in § 3.3 and r is the atomic radius (Appendix A). The calculated RPI for Fe matrix is compared with those by Bogaerts and Gijbels [3] in Table 1 and Fig. 4(a). The ratio of RPI of eq.(8) over their RPI varies from 0.45 (B) to its maximum of 1.66 (Cr, Mo). The ratio of RPI over those in ref. [3] for Fe matrix takes its minimum of 0.3 (C). Replacement of the atomic radii by those from ref. [19] in eq.(8) does not improve the situation, the ratio of new RPI values over those in ref. [3] for Fe matrix varies from the minimum of 0.58 (C) to the maximum of 2.22 (Ca). Hence, the discrepancy between the present calculation (eq.(8)) and that in ref. [3] is not simply due to the different choice of the atomic radii, because the RT values calculated with the atomic radii from ref. [19] agree with those in ref. [3], as mentioned in § 3.3. RPI calculation in ref. [3] is based on the rate equation, incorporating Ar metastable (Ar*) production processes by impacts of fast electron, fast Ar ion, fast Ar atom and etc., and loss processes such as ionization by fast electrons, excitation to higher energy level, electron quenching to the nearby resonant levels, Penning ionization of sputtered atoms, two- and three-body collisions with Ar ground state atoms, diffusion to and de-excitation at the walls. These calculated RPI values naturally differ from those of a simplified eq.(8).

RPI is also compared with REI for Fe matrix in Fig. 4(a). Z (atomic number of impurities)- dependence of RPI in Fe matrix is more stronger than that of REI. Recombination of ions with electrons, the details of which are discussed by Vieth and Huneke [6], will reduce the ion fraction, and modify REI and RPI. In this report, the recombination process is discarded, since the electron density is assumed to be low [3].

3.5 Extraction efficiency

Finally, we consider the relative extraction efficiency (RE) of impurity ions to that of matrix ions, which are generated near the anode by EI and/or PI. In refs. [3-4], the extraction efficiency is assumed to be independent of mass, i. e., RE = 1. In this study, $M^{-1/2}$ dependence is adopted for the extraction efficiency [29],

$$RE = (M_S / M_X)^{1/2}. \quad (9)$$

A more weaker mass dependent RE is discussed by Vieth and Huneke [6]: replacement of mass M by the reduced mass μ and/or by smaller exponent than 0.5 in eq.(9).

4. Results and discussion

The relative ion yields can be calculated with the equations described above, assuming that the detection efficiency is mass independent. The results for Fe, Cu and Al matrices are given in Tables 1-3 and Figs. 5-7. Here Ar^+ ion energy is taken as 150 eV for calculation of RS with eq.(4) and the electron energy is taken as 100 eV for REI evaluation, as discussed in § 3.2 and § 3.4.1. Since, RIY is calculated by the relative quantities (eq.(2)), the ratios of the calculated RIY (RIY-cal.) over the experimental RIY (RIY-exp.) are appropriate for comparison between the calculation and experiment.

For 33 impurities in Fe matrix, RT (relative transport efficiency), RE (relative extraction efficiency) and RT · RE range from 0.39 (B) to 2.2 (Ba), 2.8 (Li) to 0.52 (Bi) and 1.9 (Li) to 0.6 (Au), respectively, as seen in Table 1. The ratios (R-ETE = REI · RT · RE / RIY-exp.) of the RIY-cal. (REI · RT · RE) based on the electron impact ionization with RS=1 over the RIY-exp. vary from 0.5 (Pb) to 10 (Li) for 30 impurities, as seen in Fig. 5(a) and Table 1. Hence, the calculation is not satisfactory. The ratios (R-PTE) of the RIY-cal. (RPI · RT · RE) based on the Penning ionization with RS=1 over the RIY-exp. vary from 0.36 (Au) to 26 (Li) for 33 impurities (Fig. 5(a) and Table 1). Thus agreement of the calculation with the experiment is worse. The ratios of the RIY-cal. by Bogaerts and Gijbels [3] over the RIY-exp. scatter from 0.68 (V) to 7.4 (Na). Their calculation is neither satisfactory, as described in § 1. One reminds that the present experimental RIYs agree with those in ref. [3] within 20 %, for 26 impurities. The present RIY-exp. is larger by 50% (Be), 60% (Cd) and 30% (Au), and smaller by ~25% (Zr, Sb) and 40% (As) than those in ref. [3].

In Fe matrix, the ratios (R-SETE) of the RIY-cal. (RS · REI · RT · RE) based on EI with RS of eq.(4) over the RIY-exp. scatter between 0.2 (Ca) and 5 (Ga) for 33 impurities, as seen in Fig. 5(b) and Table 1. The ratios (R-SPTE) of the RIY-cal. (RS · RPI · RT · RE) based on

PI with RS of eq.(4) over the RIY-exp. scatter between 0.2 (B) and 13 (Na). Agreement of the calculation based on RS of eq.(4) with the experiment is neither satisfactory.

For 10 impurities (S, Fe, Co, Ni, Zn, As, Se, Ag, Sn, and Te) in Cu matrix as shown in Fig. 6(a) and Table 2, the RIY-cal. (REI · RT · RE) agree with the RIY-exp. within a factor of 2 (0.5 (Ni) to 1.9 (S)). For Pb impurity, the RIY-cal. is a little bit smaller than the RIY-exp. (R-ETE = 0.23 for Pb). Replacement of REI by RPI does not improve the agreement between the calculated and experimental RIYs. The ratios (R-PTE) vary from 0.14 (Pb) to 0.9 (Ag).

In Cu matrix (Fig. 6(b) and Table 2), the ratios (R-SETE) scatter within 0.4 to 1.2, except for Pb (0.13). The agreement becomes slightly better and thus, replacement of RS=1 by eq.(4) seems to be reasonable in this case. However, this improvement is probably fortuitous, because the data points are not enough. The ratios (R-SPTE) scatter between 0.06 and 0.9 and the agreement is poor.

The situation for Al matrix is similar to Fe matrix (Fig. 7(a) and (b) and Table 3). For 21 impurities in Al matrix, the ratios (R-ETE) scatter between 0.2 (Fe) and 1 (Ga), except for Ti (0.16) and Pb (0.11). The ratios (R-PTE) scatter between 0.3 (Pb, Sb) and 6 (Na) for 27 impurities. The ratios (R-SETE) scatter between 0.2 (Ca, Ti, Pb) and 2.4 (Ga). The ratios (R-SPTE) scatter between 0.3 (B) and 11 (Na) for 27 impurities. Hence, replacement of RS=1 by eq.(4) does not improve the situation.

It also appears that replacement of M by the reduced mass in eq.(9) gives slightly better agreement between RIY-cal. and RIY-exp. especially for impurities with low and high atomic numbers such as Li and Pb.

5. Summary

In conclusion, the present simple calculation reproduces RIYs as good as those of theory in ref. [3]. However, the agreement between the calculation and experiment is not satisfactory at present. Summarising specifically,

(1) The relative sputtering yield RS is reasonably set equal to 1, unless strong segregation takes place. Segregation is to be investigated.

(2) The relative transport efficiency RT varies within a factor of ~2. The relative extraction efficiency RE also varies within a factor of ~2. RE can be replaced by a more moderate mass-dependent formula than eq.(9) or unity.

(3) The most important process in GDMS is the ionization of sputtered atoms near the anode, as already pointed out in ref. [3]. The electron energy distribution near the anode is necessary for the case that the electron impact ionization is dominant. Data of electron impact

ionization cross section for Sb, Bi, Pd, Rh, Pt and Au are desired. The Penning ionization cross sections are of crucial importance. The choice of atomic radii in eq.(8) is also to be examined. Asymmetric or quasi-symmetric charge transfer may play role [3], though the data is scarce.

It has been pointed out that the following quantities in GD are not well known:
(1) Energy of Ar ions and Ar neutral responsible for sputtering of the cathode (target) and the current (flux) of these energetic ions and atoms,
(2) Electron energy distribution and the electron current near the anode,
(3) Metastable Ar* density.

Many of processes in GDMS are common in plasma physics and plasma-wall interactions. More systematic investigations, especially the ionization process would be fruitful to improve the theory.

References
(1) B. Chapman, *Glow Discharge Processes*, John Wiley & Sons, 1980.
(2) W. W. Harrison, J. Analytical Atomic Spectrometry 3(1988)867.
(3) A. Bogaerts and R. Gijbels, J. Anal. Atomic Spectrometry 11(1996)841.
(4) A. Bogaerts, Mathematical modeling of a direct current glow discharge in argon, Ph. D. Thesis, 1996, University of Antwerp.
(5) W. Vieth and J.C. Huneke, Spectrochim. Acta 45B(1990)941.
(6) W. Vieth and J.C. Huneke, Spectrochim. Acta 46B(1991)137.
(7) E. S. Beary and P. J. Paulsen, Anal. Chem. 67(1995)3139.
(8) E. W. Eckstein, J. W. Coburn and E. Kay, Int. J. Mass Spectrometry and Ion Physics 17(1975)129.
(9) R. Behrisch, *Sputtering by Particle Bombardment*, (Springer-Verlag, 1981).
(10) J. F. Ziegler, J. P. Biersack and U. Littmark, *The Stopping and Ranges of Ions in Solids* (Pergamon, 1985).
(11) N. Matsunami et al., Atomic Data and Nuclear Data Tables 31(1984)1.
(12) Y. Yamamura and H. Tawara, Atomic Data and Nuclear Data Tables 62(1996)149.
(13) M. van Straaten, A. Bogaerts and R. Gijbels, Spectrochimica Acta 50(1995)583.
(14) S. Born (Ph D. Thesis, 1999 and private communication).
(15) C. Jonkers, Analyse van Metalen en Metaaloppervlakken met Glimontladings-massaspectrometrie (Analysis of metal and metal-alloys in glow discharge mass spectrometry), Ph. D. Thesis, 1995, University of Antwerp.
(16) R. Shimizu, Nucl. Instrum. & Methods B18 (1987)486.
(17) W. Hang and W. W. Harrison, Anal. Chem. 69(1997)4957.
(18) T. A. Carlson, C. C. Lu, T. C. Tucker, C. W. Nester Jr. and F. B. Malik, Report ORNL-4614(1970)
(19) C. Kittel, *Introduction to Solid State Physics*, 6th edition (John Wiley & Sons Inc. 1986).
(20) For atoms with s and p orbitals as the outer shell, r is reasonably given by $(n_s r_c(s)+n_p r_c(p))/(n_s+n_p)$, n_s and n_p being the number of electrons in s- and p-shells, and $r_c(s)$ and $r_c(p)$ are the calculated atomic radius of s- and p-shells, respectively[18]. For atoms having unfilled d-shells, d-shell contribution can be incorporated into $r = (n_s r_c(s)+n_d r_c(d))/(n_s+n_d)$. Here, n_d is taken as 1 when the number of total d-electrons is less than 5 and 0.5 for other cases, considering the energy difference between s- and d-orbitals.
(21) P. E. Siska, Rev. Mod. Phys. 65(1993)337.
(22) ICRU report 37, Stopping Powers for Electrons and Positrons, (1984, USA).
(23) K. L. Bell, H. B. Gilbody, J. G. Hughes, A. E. Kingston and F. J. Smith, J. Phys. Chem. Ref. Data 12(1983)891.
(24) M. A. Lennon, K. L. Bell, H. B. Gilbody, J. G. Hughes, A. E. Kingston, M. J. Murray and F. J. Smith, J. Phys. Chem. Ref. Data 17(1988)1285.
(25) M. J. Higgins, M. A. Lennon, J. G. Hughes, K. L. Bell, H. B. Gilbody, A. E. Kingston and F. J. Smith, CLM-R294 (Culham Laboratory, UK, 1989).
(26) H. Tawara, NIFS-DATA-51 (1999).
(27) R. L. Smith, D. Serxner and K. R. Hess, Anal. Chem. 61(1989)1103.
(28) L. A. Riseberg, W. F. Parks and L.D. Schearer, Phys. Rev. 8(1973)1962.
(29) S. Humphries, Jr., *Charged Particle Beams*, John Wiley & Sons, 1990.

Appendix A Atomic number(Z), mass(M), density(g/cm³), surface binding energy(U), ionization potential(I), sputtering yield(S) of elemental target for 150 eV Ar impact, electron impact ionization cross section(EICS) in 10^{-16}cm² at 100 eV and atomic radius(r).

	Z	M	g/cm³	U(eV)	I(eV)	S	EICS	r(nm)
Li	3	6.94	0.530	1.63	5.39	0.0644	1.45	0.1985
Be	4	9.01	1.80	3.32	9.32	0.150	1.91	0.1381
B	5	10.81	2.35	5.77	8.30	0.0740	2.03	0.1072
C	6	12.00	2.266	7.37	11.26	0.0700	2.15	0.09137
N	7	14.00			14.54		1.56	0.07485
O	8	16.00			13.61		1.45	0.06368
Ne	10	20.00			21.56		0.680	0.04940
Na	11	23.00	1.00	1.11	5.14	1.54	2.10	0.2128
Mg	12	24.31	1.74	1.51	7.64	1.06	2.40	0.1652
Al	13	26.98	2.70	3.39	5.98	0.252	6.50	0.1468
Si	14	28.09	2.32	4.63	8.15	0.180	5.20	0.1266
P	15	30.97	1.82	3.43	10.55	0.195	4.40	0.1204
S	16	32.06	2.07	2.85	10.36	0.269	4.20	0.1048
Cl	17	35.45			13.01		3.30	0.09324
Ar	18	40.00			15.76		2.45	0.09243
K	19	39.10	0.863	0.934	4.34	0.224	4.90	0.2614
Ca	20	40.08	1.54	1.84	6.11	0.210	3.20	0.2101
Sc	21	44.96	3.00	3.90	6.56	0.186	11.5	0.1961
Ti	22	47.90	4.52	4.85	6.83	0.230	3.50	0.1856
V	23	50.94	6.10	5.31	6.74	0.292	8.75	0.1771
Cr	24	52.00	7.19	4.10	6.76	0.520	4.00	0.1883
Mn	25	54.94	7.43	2.92	7.43	0.839	4.15	0.1633
Fe	26	55.85	7.87	4.28	7.90	0.536	3.70	0.1576
Co	27	58.93	8.80	4.39	7.86	0.605	5.00	0.1524
Ni	28	58.71	8.90	4.44	7.63	0.635	2.60	0.1477
Cu	29	63.54	8.95	3.49	7.72	0.869	2.30	0.1591
Zn	30	65.37	7.11	1.35	9.39	1.912	2.80	0.1394
Ga	31	69.72	5.91	2.81	6.00	0.715	6.90	0.1389
Ge	32	72.59	5.34	3.85	7.88	0.454	5.80	0.1273
As	33	74.92	5.72	2.96	9.81	0.670	5.25	0.1291
Se	34	78.96	4.79	2.25	9.75	0.724	5.30	0.1162
Kr	36	83.80			14.00		3.40	0.09847
Rb	37	85.47	1.53	0.852	4.18	0.547	4.60	0.2750
Sr	38	87.62	2.60	1.72	5.69	0.476	4.18	0.2258
Y	39	88.91	4.49	4.37	6.50	0.339		0.2077
Zr	40	91.22	6.47	6.25	6.95	0.298	5.23	0.1957
Nb	41	92.91	8.60	7.57	6.77	0.303		0.2012
Mo	42	95.94	10.21	6.82	7.18	0.432	6.05	0.1935
Ru	44	101.10	12.18	6.74	7.36	0.483	4.87	0.1815
Rh	45	102.90	12.40	5.75	7.46	0.594		0.1767
Pd	46	106.40	11.96	3.89	8.33	0.828		0.173
Ag	47	107.87	10.47	2.95	7.57	1.01	2.60	0.1683
Cd	48	112.40	8.58	1.16	8.99	1.81	4.43	0.1505
In	49	114.82	7.31	2.52	5.78	0.777	7.90	0.1516
Sn	50	118.70	7.28	3.14	7.34	0.636	7.3	0.1418
Sb	51	121.75	6.62	2.75	8.64	0.619		0.1331
Te	52	127.60	6.22	2.23	9.01	0.698	8.83	0.1345
Xe	54	131.30			12.13		4.45	0.1171
Ba	56	137.34	3.52	1.90	5.21	0.432	4.80	0.2495
W	74	183.90	19.29	8.90	7.98	0.382		0.1669
Re	75	186.20	21.04	8.03	7.87	0.471		0.1609
Pt	78	195.10	21.40	5.84	8.96	0.624		0.1544
Au	79	197.00	19.30	3.81	9.22	0.862	14.0	0.1505
Tl	81	204.40	11.88	1.88	6.11	0.949	7.20	0.1796
Pb	82	207.20	11 32	2.03	7.41	0.838	4.35	0.1576
Bi	83	208.98	9.81	2.18	7.29	0.642		0.1675

Table 1 Comparison of the calculated relative ion yield (RIY) with the experimenral RIY (RIY-exp) in Fe matrix. RSF-exp is the experimental relative sensitivity factor. REI, RPI, RT and RE are the calculated values of the relative electron-impact-ioniztion cross-section of impurity to that of Fe (matrix) at 100 eV (eq.(6)), the relative Penning ionization cross section (eq.(8)), the relative transport efficiency (eq.(5)) and the relative extraction efficiency (eq.(9)). RS is the relative sputtering yield of impurity to that of Fe by 150 eV Ar impact at normal incidence (eq.(4)). R-ETE and R-PTE are the ratios of REI · RT · RE and RPI · RT · RE over RIY-exp, respectively. Similary, R-SETE and R-SPTE are the ratios of RS · REI · RT · RE and RS · RPI · RT · RE over RIY-exp, respectively. RPI(BG96) and RIY(BG96) are the calculated RPI and RIY taken from Bogaerts and Gijbels [3].

	RSF-exp	RIY-exp	REI	RPI	RPI(BG96)	RT	RE	RTxRE	REIxRTxRE	RIY(BG96)	R-ETE	R-PTE	RS	R-SETE	R-SPTE
Fe			1.00	1.00	1.00	1.000	1.00	1.000	1.00	1.00			1.00	1.00	1.00
Li	1.67	0.0744	0.392	1.01	0.640	0.6820	2.84	1.935	0.758	0.390	10.2	26.2	0.0458	0.466	1.20
Be	1.53	0.105	0.516	0.378	0.500	0.4775	2.49	1.188	0.614	0.260	5.82	4.28	0.217	1.26	0.925
B	1.29	0.150	0.549	0.190	0.420	0.3852	2.27	0.8756	0.480	0.190	3.20	1.11	0.186	0.596	0.207
Na	2.03	0.203	0.588	1.95	1.30	1.180	1.56	1.838	1.04	1.50	5.14	17.7	0.745	3.83	13.2
Mg	1.54	0.283	0.649	0.928	1.05	0.8562	1.52	1.296	0.841	1.04	2.97	4.25	0.698	2.08	2.97
Al	1.38	0.350	1.76	0.672	0.940	0.7612	1.44	1.095	1.92	0.880	5.50	2.10	0.372	2.05	0.783
Si	1.85	0.272	1.41	0.436	0.780	0.6457	1.41	0.9105	1.28	0.820	4.71	1.46	0.363	1.71	0.531
P	3.18	0.175	1.19	0.386	0.740	0.6270	1.34	0.8421	1.00	0.570	5.71	1.85	0.292	1.66	0.540
S	3.90	0.147	1.14	0.257	0.740	0.5437	1.32	0.7177	0.815	0.570	5.53	1.25	0.334	1.85	0.419
Ca	0.550	1.30	0.865	2.20	1.58	1.357	1.18	1.602	1.39	2.18	1.06	2.70	0.168	0.179	0.454
Ti	0.480	1.79	0.946	1.58	1.14	1.196	1.08	1.291	1.22	1.25	0.684	1.14	0.466	0.332	0.555
V	0.560	1.63	2.36	1.39	1.08	1.139	1.05	1.193	2.82	1.10	1.73	1.02	0.676	1.17	0.689
Cr	2.21	0.421	1.08	1.68	1.01	1.242	1.04	1.287	1.39	1.01	3.30	5.13	0.929	3.07	4.77
Mn	1.48	0.674	1.12	1.11	0.990	1.043	1.01	1.051	1.18	0.980	1.75	1.73	1.07	1.87	1.85
Co	1.10	0.959	1.35	0.914	1.00	0.9695	0.974	0.9438	1.28	1.01	1.33	0.900	1.16	1.54	1.04
Ni	1.51	0.696	0.703	0.832	1.00	0.9319	0.975	0.9089	0.639	1.00	0.917	1.09	1.23	1.13	1.33
Cu	5.14	0.221	0.622	1.06	1.04	1.039	0.938	0.9737	0.805	1.08	2.73	4.64	1.32	3.62	6.14
Zn	5.77	0.203	0.767	0.714	1.13	0.8871	0.924	0.8200	0.621	1.25	3.06	2.89	1.12	3.44	3.24
Ga	4.56	0.274	1.86	0.715	1.12	0.8939	0.895	0.8001	1.49	1.24	5.45	2.09	0.876	4.77	1.83
As	5.06	0.284	1.42	0.581	1.05	0.8304	0.863	0.7169	1.02	1.10	3.85	1.58	0.864	3.33	1.36
Se	3.26	0.434	1.43	0.428	0.980	0.7431	0.841	0.6250	0.895	0.980	2.06	0.617	0.710	1.47	0.438
Zr	0.850	1.92	1.41	2.09	1.42	1.451	0.782	1.135	1.50	1.90	0.835	1.24	0.812	0.678	1.00
Mo	1.12	1.53	1.64	2.04	1.23	1.439	0.763	1.098	1.80	1.48	1.17	1.46	1.28	1.50	1.67
Ag	4.31	0.448	0.703	1.38	1.30	1.217	0.720	0.8755	0.615	1.62	1.37	2.66	1.30	1.78	3.46
Cd	5.71	0.352	1.20	0.980	1.39	1.062	0.705	0.7487	0.898	1.83	2.54	2.08	0.915	2.33	1.90
In	3.95	0.620	2.14	1.00	1.44	1.075	0.697	0.7495	1.60	1.96	3.07	1.45	0.854	2.62	1.23
Sn	2.47	0.880	1.97	0.825	1.46	0.9943	0.686	0.6820	1.35	2.01	1.56	0.654	0.871	1.36	0.589
Sb	6.26	0.414		0.685	1.50	0.9247	0.677	0.6263		2.11		1.03	0.742		0.788
Te	3.46	0.660	2.39	0.711	1.33	0.9416	0.662	0.6230	1.49	1.71	2.25	0.670	0.679	1.53	0.455
Ba	1.17	2.10	1.30	4.57		2.156	0.638	1.375	1.78		0.849	2.99	0.358	0.304	1.07
Au	2.02	1.75		1.04	1.38	1.128	0.532	0.6003		1.84		0.358	1.43		0.512
Pb	2.58	1.45	1.18	1.20	1.75	1.199	0.519	0.6227	0.732	2.78	0.505	0.515	0.742	0.375	0.382
Bi	4.05	0.924		1.44	1.84	1.297	0.517	0.6706		3.06		1.05	0.610		0.638

Table 2 Similar to Table 1, except for Cu matrix.

	RSF-exp	RIY-exp	REI	RPI	RT	RE	RTxRE	REIxRTxRE	RPIxRTxRE	R-ETE	R-PTE	RS	R-SETE	R-SPTE
Cu			1.00	1.00	1.00	1.00	1.00	1.00	1.00			1.00		
P	0.650	0.752	1.91	0.365	0.604	1.43	0.865	1.65	0.318	2.20	0.420	0.221	0.484	0.0927
S	0.710	0.708	1.83	0.243	0.524	1.41	0.737	1.35	0.179	1.80	0.253	0.253	0.482	0.0640
Fe	0.270	3.20	1.81	0.947	0.963	1.07	1.03	1.85	0.973	0.517	0.304	0.758	0.391	0.230
Co	0.290	3.20	2.17	0.866	0.933	1.04	0.969	2.10	0.839	0.657	0.282	0.876	0.576	0.230
Ni	0.440	2.10	1.13	0.788	0.897	1.04	0.933	1.05	0.735	0.502	0.350	0.930	0.467	0.325
Zn	1.35	0.762	1.22	0.676	0.854	0.988	0.842	1.03	0.570	1.35	0.747	0.850	1.15	0.635
As	1.05	1.12	2.28	0.551	0.799	0.921	0.736	1.68	0.405	1.50	0.362	0.653	0.979	0.236
Se	0.880	1.40	2.30	0.405	0.715	0.897	0.642	1.48	0.260	1.05	0.186	0.537	0.566	0.0998
Ag	1.32	1.29	1.13	1.29	1.17	0.767	0.899	1.02	1.16	0.788	0.900	0.982	0.774	0.884
Sn	0.710	2.63	3.17	0.782	0.957	0.732	0.700	2.22	0.547	0.844	0.208	0.658	0.556	0.137
Sb	1.22	1.57		0.848	0.890	0.722	0.643		0.417		0.286	0.561		0.148
Te	0.960	2.09	3.84	0.673	0.907	0.708	0.640	2.46	0.431	1.18	0.208	0.513	0.603	0.106
Pb	0.630	5.19	1.89	1.14	1.15	0.554	0.639	1.21	0.726	0.233	0.140	0.561	0.131	0.0785
Si	1.34	2.45		1.36	1.25	0.551	0.689		0.940		0.384	0.461		0.177

Table 3 Similar to Table 2, except for Al matrix.

	RSF-exp	RIY-exp	REI	RPI	RT	RE	RTxRE	REIxRTxRE	RPIxRTxRE	R-ETE	R-PTE	RS	R-SETE	R-SPTE
Al			1.00	1.000	1.000	1.00	1.000	1.000	1.000			1.00		
Be	0.580	0.576	0.294	0.552	0.627	1.73	1.09	0.319	0.611	0.554	1.06	0.583	0.323	0.618
B	1.03	0.391	0.312	0.283	0.506	1.58	0.800	0.250	0.226	0.639	0.579	0.500	0.319	0.289
Na	1.00	0.852	0.323	2.90	1.55	1.08	1.68	0.542	4.87	0.636	5.71	2.00	1.27	11.4
Mg	0.870	1.03	0.369	1.38	1.12	1.05	1.18	0.437	1.63	0.424	1.59	1.87	0.795	2.97
Si	1.41	0.739	0.800	0.649	0.848	0.980	0.831	0.685	0.540	0.900	0.730	0.976	0.878	0.712
P	1.57	0.730	0.677	0.574	0.824	0.933	0.769	0.520	0.442	0.713	0.605	0.783	0.558	0.474
Ca	0.900	1.66	0.492	3.27	1.78	0.820	1.46	0.720	4.78	0.434	2.88	0.452	0.198	1.30
Ti	0.450	3.99	0.538	2.35	1.57	0.751	1.18	0.635	2.77	0.159	0.686	1.31	0.208	0.907
V	0.570	3.29	1.35	2.07	1.50	0.728	1.09	1.47	2.26	0.446	0.686	1.82	0.809	1.24
Cr	1.35	1.43	0.615	2.50	1.63	0.720	1.17	0.723	2.94	0.508	2.05	2.50	1.26	5.13
Mn	1.03	1.97	0.638	1.85	1.37	0.701	0.960	0.613	1.58	0.311	0.804	2.87	0.892	2.31
Fe	0.850	2.42	0.569	1.49	1.31	0.695	0.913	0.520	1.36	0.215	0.562	2.89	0.577	1.51
Co	0.810	2.69	0.769	1.38	1.27	0.677	0.862	0.663	1.17	0.246	0.438	3.11	0.766	1.36
Ni	1.39	1.57	0.400	1.24	1.22	0.678	0.830	0.332	1.03	0.211	0.654	3.30	0.698	2.16
Cu	3.83	0.600	0.354	1.57	1.36	0.662	0.889	0.315	1.40	0.524	2.33	3.55	1.86	8.27
Zn	3.18	0.762	0.431	1.06	1.17	0.642	0.749	0.323	0.796	0.423	1.04	3.02	1.28	3.15
Ga	3.35	0.773	1.06	1.06	1.17	0.622	0.731	0.776	0.777	1.00	1.01	2.35	2.36	2.36
Zr	1.02	3.33	0.805	3.11	1.91	0.544	1.04	0.834	3.23	0.250	0.989	2.18	0.546	2.11
Mo	1.04	3.42	0.931	3.03	1.89	0.530	1.00	0.933	3.04	0.273	0.889	3.45	0.941	3.07
Ag	4.16	0.982	0.400	2.03	1.60	0.500	0.798	0.320	1.52	0.332	1.89	3.47	1.15	5.85
Cd	3.48	1.20	0.682	1.46	1.40	0.490	0.684	0.466	0.897	0.388	0.831	2.46	0.954	2.04
In	3.95	1.08	1.22	1.49	1.41	0.485	0.684	0.836	1.02	0.774	0.947	2.29	1.77	2.17
Sn	2.20	2.00		1.23	1.31	0.477	0.623		0.785		0.382	2.34		0.894
Sb	2.46	1.83		1.02	1.21	0.471	0.572		0.583		0.318	1.89		0.634
Au	4.91	1.49		1.55	1.48	0.370	0.548		0.849		0.569	3.84		2.19
Pb	2.16	3.58	0.669	1.78	1.58	0.361	0.589	0.381	1.01	0.107	0.285	1.99	0.213	0.568
Bi	3.69	2.10		2.14	1.70	0.358	0.612		1.31		0.625	1.84		1.02

Fig. 1. Schematics of glow discharge after Chapman [1]; (a) subdivision of the glow discharge into different regions, (b) luminous intensity, (c) potential, (d) electric field, (e) space charge density and (f) current density.
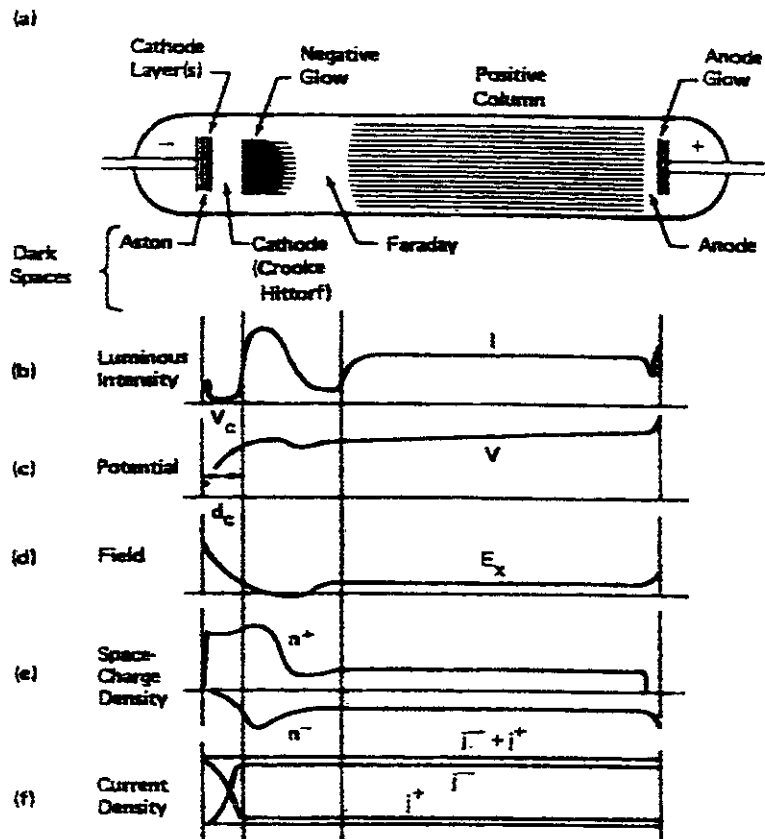

Fig. 2. Ratio of the sputtering yields S calculated by TRIM1997 over the experimental S for various elemental targets as a function of Ar^+ energy at normal incidence.
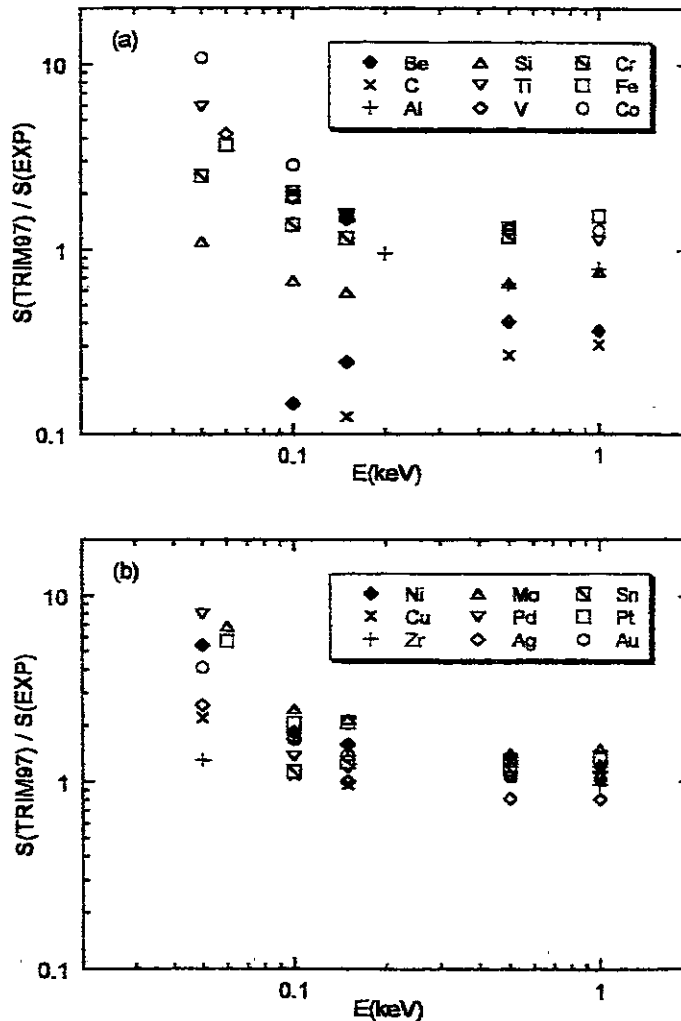
Fig. 3. Ratio of the sputtering yields of elements with the atomic number Z over that of Cu by Ar⁺ with 50 - 500 eV. The sputtering yields are calculated by TRIM(1997 version) at normal incidence.
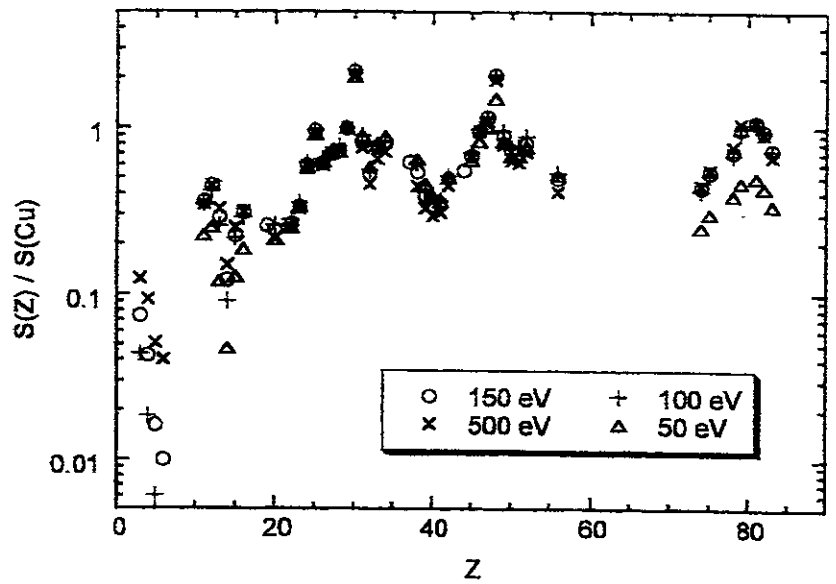
Fig. 4. Ratio of the electron impact ionization cross section (EICS) of elements with the atomic number Z over that of Fe (a) and Cu (b). The calculated ratios of PI (Penning ionization) cross section of eq.(8) ($\triangle$) and those from [3] ($\square$, RPI (BG96)) are also shown in Fig. 4(a).
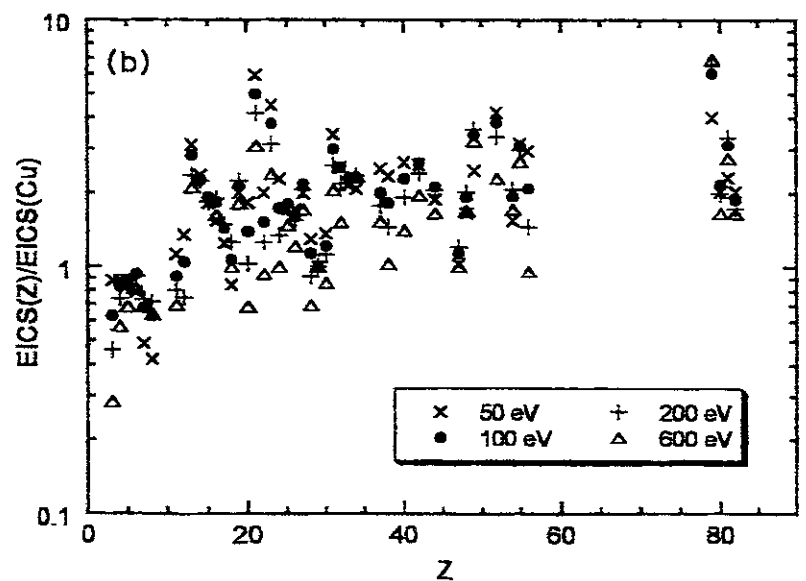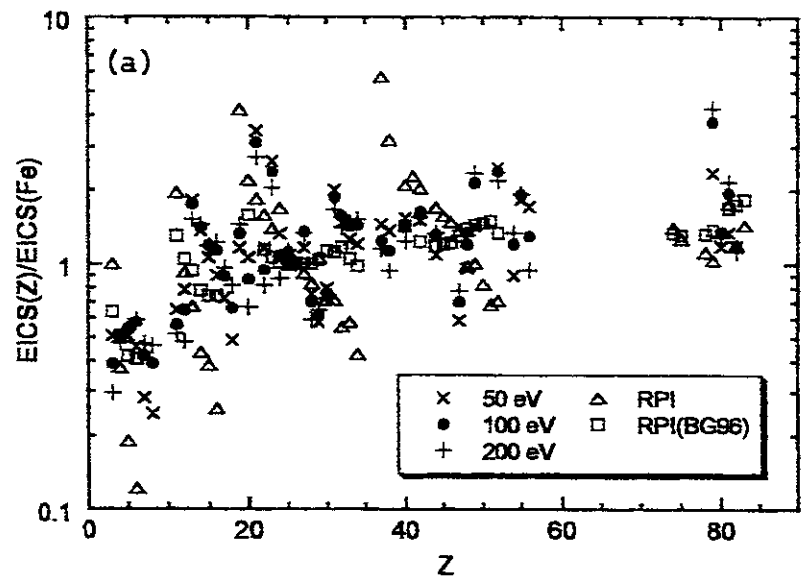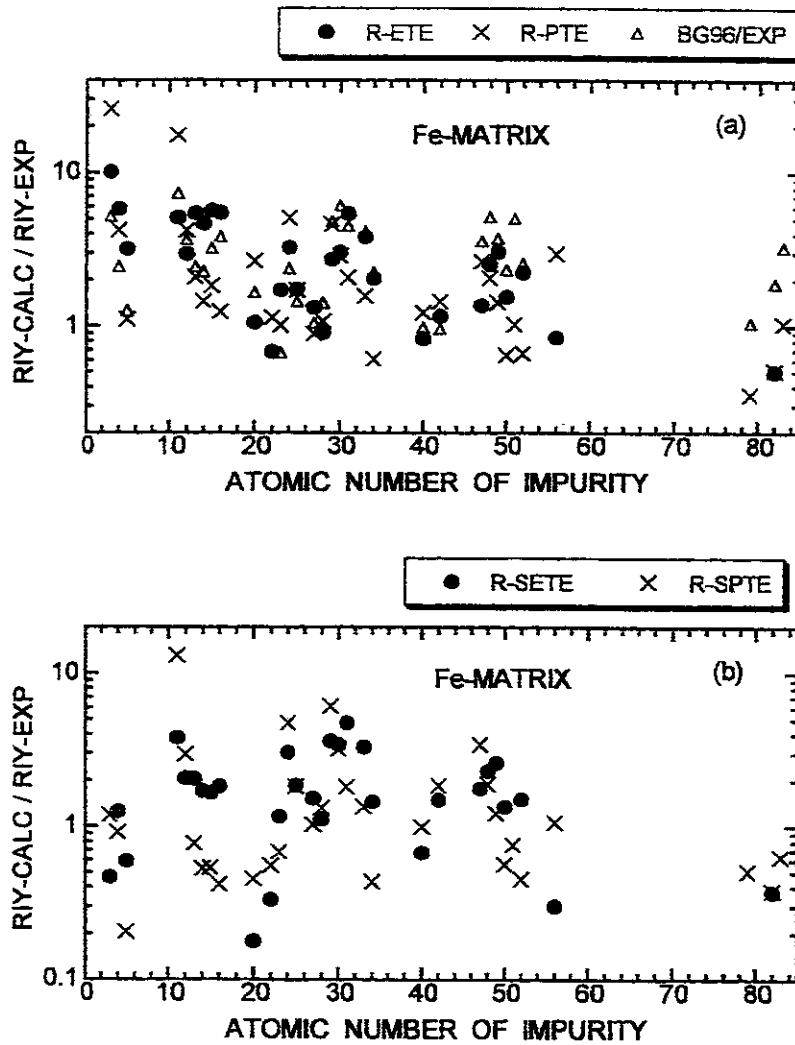
Fig. 5(a) Ratios of the calcualted relative ion yield (RIY-CALC) over the experimental (RIY-EXP) vs atomic number of impurities in Fe matrix. R-ETE and R-PTE are REI · RT · RE and RPI · RT · RE over RIY-EXP, respectively (see also Table 1). BG96/EXP is the ratio of the RIY-CALC taken from ref. [3] over the RIY-EXP.
(b) Ratios of RIY-CALC over RIY-EXP vs atomic number of impurities in Fe matrix. R-SETE and R-SPTE are RS · REI · RT · RE and RS · RPI · RT · RE over RIY-EXP, respectively (see Table 1).

Fig. 6(a) and (b) Similar to Fig. 5(a) and (b), except for Cu matrix (see Table 2).
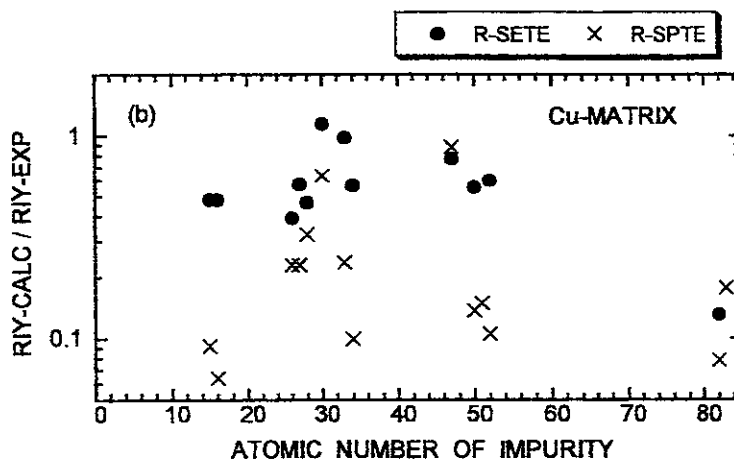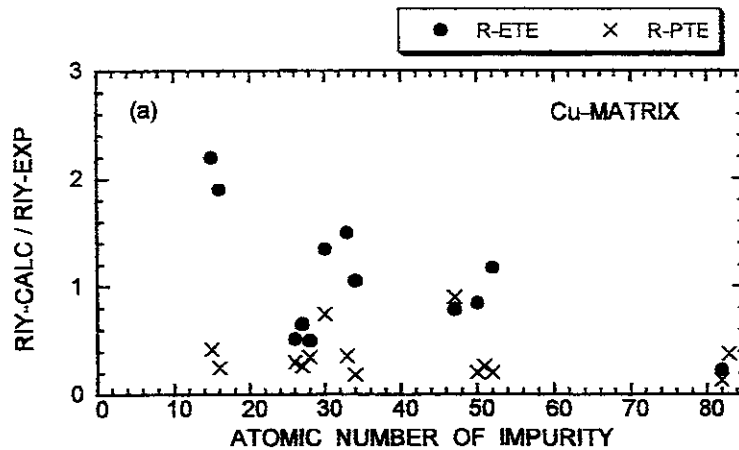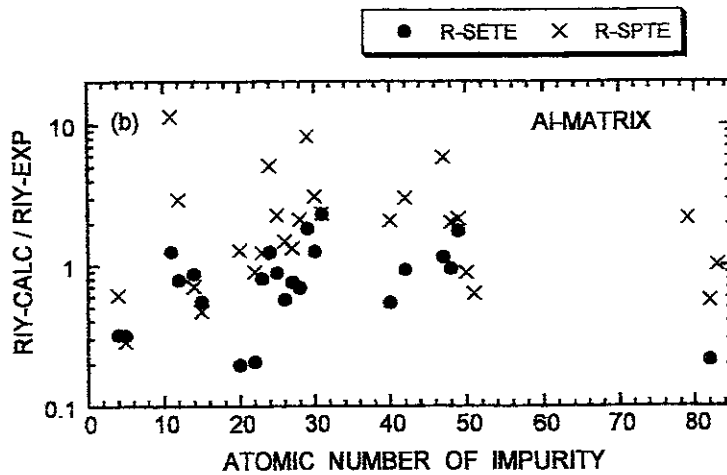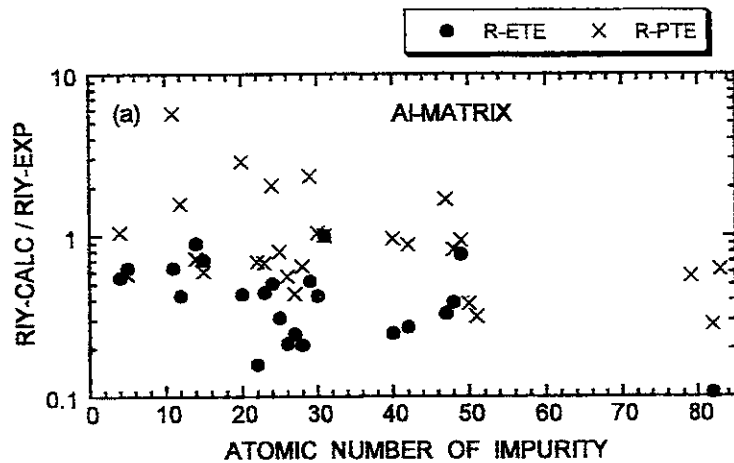
Fig. 7(a) and (b) Similar to Fig. 6(a) and (b), except for Al matrix (see Table 3).

Publication List of NIFS-DATA Series

NIFS-DATA-1   Y. Yamamura, T. Takiguchi and H. Tawara,
Data Compilation of Angular Distributions of Sputtered Atoms; Jan. 1990

NIFS-DATA-2   T. Kato, J. Lang and K. E. Berrington,
Intensity Ratios of Emission Lines from OV Ions for Temperature and Density Diagnostics ; Mar 1990 [At
Data and Nucl Data Tables 4 4(1990)133]

NIFS-DATA-3   T. Kaneko,
Partial Electronic Straggling Cross Sections of Atoms for Protons, Mar. 1990

NIFS-DATA-4   T. Fujimoto, K. Sawada and K. Takahata,
*Cross Section for Production of Excited Hydrogen Atoms Following Dissociative Excitation of Molecular
Hydrogen by Electron Impact* ; Mar. 1990

NIFS-DATA-5   H. Tawara,
*Some Electron Detachment Data for H⁻ Ions in Collisions with Electrons, Ions, Atoms and Molecules -
an Alternative Approach to High Energy Neutral Beam Production for Plasma Heating–*;Apr 1990

NIFS-DATA-6   H. Tawara, Y. Itikawa, H Nishimura, H. Tanaka and Y Nakamura,
Collision Data Involving Hydro-Carbon Molecules , July 1990 [Supplement to Nucl. Fusion 2(1992)25;
Atomic and Molecular Processes in Magnetic Fusion Edge Plasmas (Plenum, 1995) p461]

NIFS-DATA-7   H.Tawara,
Bibliography on Electron Transfer Processes in Ion-Ion/Atom/Molecule Collisions --Updated 1990–; Aug
1990

NIFS-DATA-8   U.I.Safronova, T.Kato, K.Masai, L.A Vainshtein and A.S.Shlyapzeva,
*Excitation Collision Strengths, Cross Sections and Rate Coefficients for OV, SiXI, FeXXIII, MoXXXIX by
Electron Impact ($1s^2 2s^2 - 1s^2 2s2p - 1s^2 2p^2$ Transitions)* Dec.1990

NIFS-DATA-9   T.Kaneko,
Partial and Total Electronic Stopping Cross Sections of Atoms and Solids for Protons; Dec. 1990

NIFS-DATA-10   K.Shima, N.Kuno, M Yamanouchi and H.Tawara,
*Equilibrium Charge Fraction of Ions of Z=4-92 (0.02-6 MeV/u) and Z=4-20 (Up to 40 MeV/u) Emerging
from a Carbon Foil;* Jan.1991 [AT.Data and Nucl. Data Tables 5 1(1992)173]

NIFS-DATA-11   T. Kaneko, T. Nishihara, T. Taguchi, K Nakagawa, M Murakami, M. Hosono, S. Matsushita, K. Hayase, M Moriya.
Y.Matsukuma, K.Miura and Hiro Tawara,
Partial and Total Electronic StoppingCross Sections of Atoms for a Singly Charged Helium Ion: Part I;
Mar. 1991

NIFS-DATA-12   Hiro Tawara,
*Total and Partial Cross Sections of Electron Transfer Processes for Be^{q+} and B^{q+} Ions in Collisions with
H, H_2 and He Gas Targets -Status in 1991-;* June 1991

NIFS-DATA-13   T. Kaneko, M. Nishikori, N. Yamato, T. Fukushima, T. Fujikawa, S. Fujita, K Miki, Y. Mitsunobu, K. Yasuhara, H Yoshida
and Hiro Tawara,
Partial and Total Electronic Stopping Cross Sections of Atoms for a Singly Charged Helium Ion : Part II;
Aug. 1991

NIFS-DATA-14   T. Kato, K. Masai and M. Arnaud,
Comparison of Ionization Rate Coefficients of Ions from Hydrogen through Nickel : Sep 1991

NIFS-DATA-15   T. Kato, Y. Itikawa and K Sakimoto,
Compilation of Excitation Cross Sections for He Atoms by Electron Impact; Mar 1992

NIFS-DATA-16   T. Fujimoto, F. Koike, K. Sakimoto, R. Okasaka, K Kawasaki, K. Takiyama, T. Oda and T. Kato.
Atomic Processes Relevant to Polarization Plasma Spectroscopy ; Apr. 1992

NIFS-DATA-17   H. Tawara,

Electron Stripping Cross Sections for Light Impurity Ions in Colliding with Atomic Hydrogens Relevant to Fusion Research; Apr. 1992

NIFS-DATA-18   T. Kato,
Electron Impact Excitation Cross Sections and Effective Collision Strengths of N Atom and N-Like Ions -A Review of Available Data and Recommendations- ; Sep. 1992 [Atomic Data and Nuclear Data Tables, 57, 181-214   (1994)]

NIFS-DATA-19   Hiro Tawara,
Atomic and Molecular Data for H_2O, CO & CO_2 Relevant to Edge Plasma Impurities, Oct 1992

NIFS-DATA-20   Hiro. Tawara,
Bibliography on Electron Transfer Processes in Ion-Ion/Atom/Molecule Collisions -Updated 1993-; Apr. 1993

NIFS-DATA-21   J. Dubau and T. Kato,
Dielectronic Recombination Rate Coefficients to the Excited States of C I from C II; Aug. 1994

NIFS-DATA-22   T. Kawamura, T. Ono, Y. Yamamura,
Simulation Calculations of Physical Sputtering and Reflection Coefficient of Plasma-Irradiated Carbon Surface; Aug. 1994 [J. Nucl. Mater., 220 (1995) 1010]

NIFS-DATA-23   Y. Yamamura and H. Tawara,
Energy Dependence of Ion-Induced Sputtering Yields from   Monoatomic Solids at Normal Incidence;
Mar. 1995 [At. Data and Nucl. Data Tables, 62 (1996) 149]

NIFS-DATA-24   T. Kato, U. Safronova, A. Shlyaptseva, M. Cornille, J. Dubau,
Comparison of the Satellite Lines of H-like and He-like Spectra; Apr. 1995 [Atomic Data and Nuclear Data Tables, 67., 225 (1997)]

NIFS-DATA-25   H. Tawara,
Roles of Atomic and Molecular Processes in Fusion Plasma Researches - from the cradle (plasma production) to the grave (after-burning) -; May 1995

NIFS-DATA-26   N. Toshima and H. Tawara
Excitation, Ionization, and Electron Capture Cross Sections of Atomic Hydrogen in Collisions with Multiply Charged Ions; July 1995

NIFS-DATA-27   V.P. Shevelko, H. Tawara and E.Salzborn,
Multiple-Ionization Cross Sections of Atoms and Positive Ions by Electron Impact; July 1995 [Suppl. Nucl Fusion, 6 (1996) 101]

NIFS-DATA-28   V.P. Shevelko and H. Tawara,
Cross Sections for Electron-Impact Induced Transitions Between Excited States in He: n, n'=2,3 and 4; Aug. 1995 [Suppl. Nucl. Fusion, 6 (1996) 27]

NIFS-DATA-29   U.I. Safronova, M.S. Safronova and T. Kato,
Cross Sections and Rate Coefficients for Excitation of $\Delta n = 1$ Transitions in Li-like Ions with 6<Z<42; Sep. 1995 [Physica Scripta, 54, 68-84 (1996)]

NIFS-DATA-30   T. Nishikawa, T. Kawachi, K. Nishihara and T. Fujimoto,
Recommended Atomic Data for Collisional-Radiative Model of Li-like Ions and Gain Calculation for Li-like Al Ions in the Recombining Plasma; Sep. 1995

NIFS-DATA-31   Y. Yamamura, K. Sakaoka and H. Tawara,
Computer Simulation and Data Compilation of Sputtering Yield by Hydrogen Isotopes ($^1H^+$, $^2D^+$, $^3T^+$) and Helium ($^4He^+$) Ion Impact from Monatomic Solids at Normal Incidence; Oct. 1995

NIFS-DATA-32   T. Kato, U. Safronova and M. Ohira,
Dielectronic Recombination Rate Coefficients to the Excited States of CII from CIII; Feb. 1996 [Physica Scripta, 53, 461-472 (1996), Physica Scripta, 55, 185-199 (1997)]

NIFS-DATA-33   K.J. Snowdon and H. Tawara,
Low Energy Molecule-Surface Interaction Processes of Relevance to Next-Generation Fusion Devices:

Mar. 1996 [Comm. At. Mol. Opt. Phys. 34 (1998) 21]

NIFS-DATA-34   T Ono, T. Kawamura, K. Ishii and Y. Yamamura,
Sputtering Yield Formula for B₄C Irradiated with Monoenergetic Ions at Normal Incidence; Apr 1996 [J Nucl. Mater., 232 (1996) 52]

NIFS-DATA-35   I. Murakami, T. Kato and J. Dubau,
UV and X-Ray Spectral Lines of Be-Like Fe Ion for Plasma Diagnostics; Apr. 1996 [Physica Scripta, 54, 463-470 (1996)]

NIFS-DATA-36   K. Moribayashi and T. Kato,
Dielectronic Recombination of Be-like Fe Ion; Apr. 1996 [Physca Scripta. Vol.55, 286-297 (1997)]

NIFS-DATA-37   U. Safronova, T. Kato and M. Ohira,
Dielectronic Recombination Rate Coefficients to the Excited States of CIII from CIV; July 1996 [J. Quant Spectrosc. Radiat. Transfer, 58, 193 - 215, (1997)]

NIFS-DATA-38   T. Fujimoto, H. Sahara, G. Csanak and S. Grabbe,
Atomic States and Collisional Relaxation in Plasma Polarization Spectroscopy: Axially Symmetric Case; Oct. 1996

NIFS-DATA-39   H. Tawara (Ed.)
Present Status on Atomic and Molecular Data Relevant to Fusion Plasma Diagnostics and Modeling; Jan 1997

NIFS-DATA-40   Inga Yu. Tolstikhina,
LS-Averaged 1/Z Method as a Tool of Studying the Interactions of Highly Charged Ions with a Metal Surface; Jan. 1997

NIFS-DATA-41   K. Moribayashi and T. Kato,
Atomic Nuclear Charge Scaling for Dielectronic Recombination to Be-like Ions; Apr. 1997

NIFS-DATA-42   H. Tawara,
Bibliography on Electron Transfer Processes in Ion-ion / Atom / Molecule Collisions -Updated 1997 -; May 1997

NIFS-DATA-43   M. Goto and T. Fujimoto,
Collisional-radiative Model for Neutral Helium in Plasma: Excitation Cross Section and Singlet-triplet Wavefunction Mixing; Oct. 1997

NIFS-DATA-44   J. Dubau, T. Kato and U.I. Safronova,
Dielectronic Recombination Rate Coefficients to the Excited States of CI From CII ; Jan 1998

NIFS-DATA-45   Y. Yamamura, W. Takeuchi and T. Kawamura,
The Screening Length of Interatomic Potential in Atomic Collisions; Mar. 1998

NIFS-DATA-46   T. Kenmotsu, T. Kawamura, T. Ono and Y. Yamamura,
Dynamical Simulation for Sputtering of B4C; Mar. 1998

NIFS-DATA-47   I. Murakami, K. Moribayashi and T. Kato,
Effect of Recombination Processes on FeXXIII Line Intensities; May 1998

NIFS-DATA-48   Zhijie Li, T. Kenmotsu, T. Kawamura, T. Ono and Y. Yamamura,
Sputtering Yield Calculations Using an Interatomic Potential with the Shell Effect and a New Local Model; Oct. 1998

NIFS-DATA-49   S. Sasaki, M. Goto, T. Kato and S. Takamura,
Line Intensity Ratios of Helium Atom in an Ionizing Plasma; Oct. 1998

NIFS-DATA-50   I. Murakami, T. Kato and U. Safronova,
Spectral Line Intensities of NeVII for Non-equilibrium Ionization Plasma Including Dielectronic Recombination Processses; Jan. 1999

NIFS-DATA-51   Hiro Tawara and Masa Kato,
Electron Impact Ionization Data for Atoms and Ions -up-dated in 1998-; Feb. 1999

NIFS-DATA-52   J.G. Wang, T. Kato and I. Murakami,
Validity of n^{-3} *Scaling Law in Dielectronic Recombination Processes*; Apr. 1999

NIFS-DATA-53   J.G. Wang, T. Kato and I. Murakami,
Dielectronic Recombination Rate Coefficients to Excited States of He from He^{+}; Apr. 1999

NIFS-DATA-54   T. Kato and E. Asano,
Comparison of Recombination Rate Coefficients Given by Empirical Formulas for Ions from Hydrogen through Nickel; June 1999

NIFS-DATA-55   H.P. Summers, H. Anderson, T. Kato and S. Murakami,
Hydrogen Beam Stopping and Beam Emission Data for LHD; Nov. 1999

NIFS-DATA-56   S Born, N. Matsunami and H. Tawara,
A Simple Theoretical Approach to Determine Relative Ion Yield (RIY) in Glow Discharge Mass Spectrometry (GDMS); Jan. 2000